Dynamics of locking of peptides onto growing amyloid fibrils

Govardhan Reddy[a], John E. Straub[b], and D. Thirumalai[a,c,1]

[a]Biophysics Program, Institute for Physical Science and Technology and [c]Department of Chemistry and Biochemistry, University of Maryland, College Park, MD 20742; and [b]Department of Chemistry, Boston University, Boston, MA 02215

Edited by José N. Onuchic, University of California at San Diego, La Jolla, CA, and approved May 8, 2009 (received for review March 6, 2009)

Sequence-dependent variations in the growth mechanism and stability of amyloid fibrils, which are implicated in a number of neurodegenerative diseases, are poorly understood. We have carried out extensive all-atom molecular dynamics simulations to monitor the structural changes that occur upon addition of random coil (RC) monomer fragments from the yeast prion Sup35 and Aβ-peptide onto a preformed fibril. Using the atomic resolution structures of the microcrystals as the starting points, we show that the RC $\rightarrow$ β-strand transition for the Sup35 fragment occurs abruptly over a very narrow time interval, whereas the acquisition of strand content is less dramatic for the hydrophobic-rich Aβ-peptide. Expulsion of water, resulting in the formation of a dry interface between 2 adjacent sheets of the Sup35 fibril, occurs in 2 stages. Ejection of a small number of discrete water molecules in the second stage follows a rapid decrease in the number of water molecules in the first stage. Stability of the Sup35 fibril is increased by a network of hydrogen bonds involving both backbone and side chains, whereas the marginal stability of the Aβ-fibrils is largely due to the formation of weak dispersion interaction between the hydrophobic side chains. The importance of the network of hydrogen bonds is further illustrated by mutational studies, which show that substitution of the Asn and Gln residues to Ala compromises the Sup35 fibril stability. Despite the similarity in the architecture of the amyloid fibrils, the growth mechanism and stability of the fibrils depend dramatically on the sequence.

all-atom simulations | amyloid growth dynamics | growth mechanism of fibrils | sequence-dependent addition process | Sup35 and Aβ-peptide

A number of neurodegenerative diseases, such as Alzheimer's and Parkinson's diseases and transmissible prion disorders are associated with the formation of amyloid protein fibrils with a characteristic β-structure. In addition to proteins directly implicated in diseases, others that are unrelated by sequence or structure also form fibrils rich in β-sheet structure (1). These observations make it urgent to understand the molecular basis of amyloid fibril formation (1–3). The structures of the amyloid fibrils share a characteristic cross-β motif (4–7) with the peptides (or the proteins) forming extended β-strands that span the length of the fibril. Depending on the sequence, the strands in a given sheet are arranged in a parallel or antiparallel manner (8, 9) and lie perpendicular to the fibril axis. The near-universal morphology of the fibrils (without consideration of strains) suggests that the global mechanism that drives their formation from monomers may be similar (3). Indeed, several variations of the nucleated polymerization mechanism (NPM) have been used to account for amyloid fibril formation (10–12). According to the NPM, fluctuations (induced by denaturation stress, for example) lead to monomer conformations that can associate with other monomers to form fluid-like oligomers. If the size of the oligomer exceeds a critical value, a nucleus forms that subsequently grows into protofilaments and fibrils. Although much less is known about the growth of mature fibrils, it is suspected that they grow by incorporating 1 monomer at a time (13). Schematically, we may depict the cascade of events leading to fibrils from aggregation of n monomers as $nM \leftrightarrow M_n + mM \rightarrow M_{nc} \rightarrow PF \rightarrow AF$ where M, PF, and AF are, respectively, monomer, protofilaments, and amyloid fibrils, and $n_c(= n + m)$ is the nucleus size.

Although the overall growth mechanism described above approximately describes the kinetics of amyloid formation, the molecular details in each of the steps is still poorly understood. Characterizing the structural changes in the various intermediates in the route to fibril formation is difficult not only because they are transiently populated (14–31) but also because there are large conformational fluctuations in the oligomers and in the monomers as they add onto a growing fiber (19, 32). The conformational transitions that occur in an unstructured monomer as it adds onto the fibril can be described by using all-atom molecular dynamics (MD) simulations, provided the structures of the fibrils are known. In this regard, great progress has been made (4, 5) in obtaining structural models of amyloid fibrils by using solid-state NMR methods (6, 7). More recently, the determination of atomic structures of a number of peptides that form cross-β microcystals has been a boon to our understanding of the factors that determine fibril formation. Taking advantage of these advances, we have performed all-atom MD simulations to describe the molecular events in the growth process of amyloid fibrils. Several experiments have suggested that the kinetics of monomer incorporation is complex but can be described by a dock-lock mechanism (19, 33–35). In this scenario, which can be rationalized by using an energy landscape perspective (36, 37), the addition of the monomer is envisioned to occur in 2 distinct global stages. In the first stage, a soluble (most likely an unstructured or partially structured) monomer docks to the fibril on a time scale τ_D. In the locking stage, that occurs with a time constant τ_L, the monomer undergoes conformational changes to adopt the structure in the fibril. The lock stage is slow because the structure of the monomer has to be commensurate with the underlying fibril morphology. Indeed, estimates from experiments (33), theory (35), and computer simulations (19) show that $\tau_L/\tau_D \gg 1$. To study the conformational changes of the amyloid growth process, we used MD simulations in explicit water to investigate the process of monomer addition onto a preformed fibril. By assuming that the growth of fibrils occurs by addition of 1 monomer at a time (13), we focused on the molecular conformational changes that occur after the monomer docks to one end of the fibril. To elucidate the general scenarios for the addition of monomers, we chose 2 fibril structures, 1 from the heptapeptide GNNQQNY in the yeast prion Sup35 and the other a hexapeptide GGVVIA from Aβ monomer (4, 5). The nearly all-polar GNNQQNY molecule, from the NQ-rich prion domain (residues 7–13) of Sup35 that can aggregate to the self-propagating [PSI^+] particle and the predominantly hydrophobic GGVVIA peptide from (residues 37–42) Aβ monomer both form fibrils in which the strands are

Author contributions: J.E.S. and D.T. designed research; G.R. and D.T. performed research; G.R. and D.T. contributed new reagents/analytic tools; G.R. and D.T. analyzed data; and G.R., J.E.S., and D.T. wrote the paper.

The authors declare no conflict of interest.

This article is a PNAS Direct Submission.

[1]To whom correspondence should be addressed. E-mail: thirum@umd.edu.

This article contains supporting information online at www.pnas.org/cgi/content/full/0902473106/DCSupplemental.

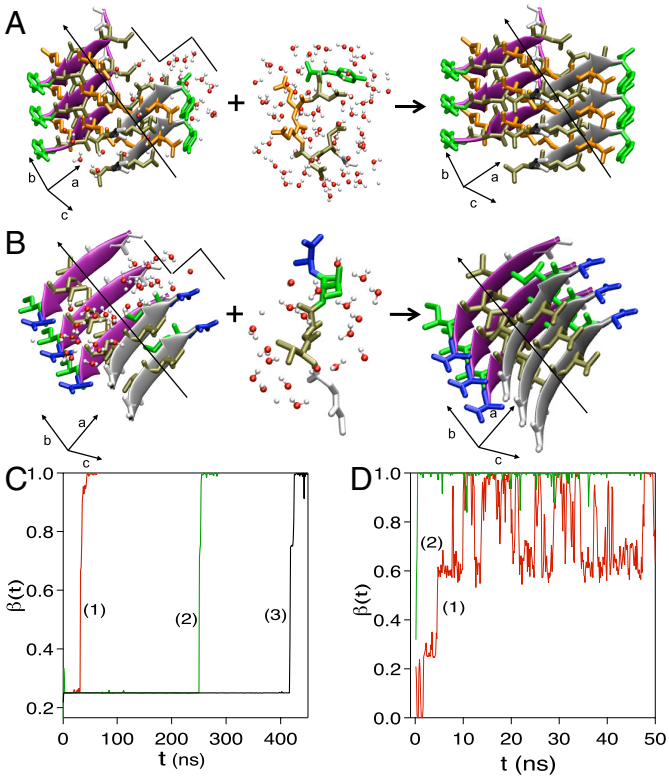

Fig. 1. Monomer addition to fibrils. (*A* and *B*) Pair of β-sheets from the Sup35 microcrystal (*A*) and Aβ microcrystal (*B*). The arrow through the crystal points toward the fibril axis (the crystal orientation labeled as (abc) is shown for clarity). One sheet is in purple and the other is shown in silver. The sheet in silver in *A* and *B* has only 2 monomers, creating a vacant position in the crystal. The missing monomer creates a terrace-like structure in the crystal. The addition of an unstructured solvated monomer leading to the fibril on the right is probed by using all-atom MD simulations. Water molecules are in the vacant part of the crystal because of the missing monomer. (*C*) Time-dependent changes in the β-strand content of the monomer, $\beta(t)$, during the locking process of Sup35 prion segment. (*D*) Same as *C* except that this is for the increase in $\beta(t)$ for the Aβ protein segment. The numbers in brackets in *C* and *D* label the trajectories.

organized as in-register parallel β-sheets. We show that the acquisition of β-strand content in both the peptides occurs cooperatively by establishing in-register interactions with the strands in the fibrils. Expulsion of water from the solvent exposed β-strand in the Sup35 fibril occurs in 2 distinct stages leading to a dry polar zipper region between the 2 sheets. Despite the qualitative similarities between the dynamics of the locking process in the 2 cases, we show that a network of hydrogen bonds between the sheets in the Sup35 fibril gives it enhanced stability compared with the Aβ fibril. We predict that substitution of the NQ-rich sequence by Ala would compromise the stability of the Sup35 fibrils.

Results and Discussion

Solvated Monomer Is a Random Coil. The isolated Sup35 prion segment peptide is predominantly in a random coil (23, 38) [Fig. 1 and supporting information (SI) Fig. S1], whereas the Aβ segment has nonnegligible β-strand content. Analysis of the structures explored by using the dihedral angles ϕ and ψ, satisfying the condition (14) for a β-strand ($-150° \le \phi \le -90°$ and $90° \le \psi \le 150°$) and for a α-helix ($-80° \le \phi \le -48°$ and $-59° \le \psi \le -27°$), show fluctuations among a number of conformations with transient secondary structure formation (Fig. S1). A conformation is in a β-strand (α-helix) if (*i*) at least 2 consecutive residues adopt strand (helix) configuration, and (*ii*) no 2 consecutive residues are in helix (β-strand) state. With this definition, the peptide GNNQQNY has negligible β-strand or α-helical content. In contrast, the Aβ-peptide, GGVVIA, has an average β-strand content of ≈0.15 with negligible propensity to form α-helix. Both peptides in isolation are predominantly random coils in water. Thus, only during the process of interaction with the fibril, the major conformational transformation from random coil to β-strand must occur.

Locking of GNNQQNY onto the Fibril Is Dynamically Cooperative. The locking process of an unstructured monomer onto a protofilament, which serves as a template, was initiated by placing the Gly residue in close proximity to the Gly on the protofilament (Fig. 1*A*) and *Methods*). The acquisition of structure in the growth process is monitored by the increase in the β-strand content of the added monomer. In the fibril structure, the residues, ^{3}NQQN^6 are in β-strand conformation as judged by the program STRIDE (39) as well as the definition based on dihedral angles, ϕ and ψ, for a β-strand (14). The equilibrium strand content for the 4 internal residues (^{3}NQQN^6) is defined as, $\beta_E = \frac{1}{4}\sum_{i=1}^{4}\delta_{i,\beta} = 1$, where $\delta_{i,\beta} = 1$ if residue i adopts the appropriate geometry for a β-strand. To probe the dynamics of changes in the monomer as it locks onto the fibril, we calculated $\beta(t) = \frac{1}{\Delta}\int_t^{t+\Delta}\beta_i(s)ds$, where $\beta_i(s) = \frac{1}{4}\sum_{i=1}^{4}\delta_{i,\beta}$ at time $t = s$ and $\Delta = 1$ ns. If the locking process is complete, we expect that at long times, the strand content of the monomer $\beta(t) \to \beta_E$. Remarkably, $\beta(t)$ changes dramatically and highly cooperatively when GNNQQNY locks onto the fibril (Fig. 1*C*) in all 3 trajectories. Analysis of the time dependence of $\beta(t)$ shows that the strand content of the locking monomer reaches 0.25 rapidly and remains at this level for duration, ranging from 30 to 425 ns depending on the trajectory (Fig. 1*C*). The additional increase in $\beta(t)$ (by ≈0.75) and the π-stacking of the Tyr ring (residue 7) occurs within 10 ns in all trajectories. The transition time, Δt, in which $\beta(t)$ increases from 0.25 to 1.0 (Fig. 1*A*) is much shorter than the trajectory-dependent first-passage time, τ_i, which is defined as the time where $\beta(\tau_i) = 1$ for the first time in the *i*th trajectory (Fig. 1*C*). The values of $\Delta t/\tau_i$ of the 3 trajectories shown are 0.16, 0.016, and 0.02, respectively, which is a reflection of the dynamic cooperativity of the locking process.

Fluctuations in $\beta(t)$ of the Aβ Peptide Persist After Locking. The increase in $\beta(t)$ upon addition of GGVVIA onto the vacant location of the underlying protofibril as a function of t also increases sharply in a small interval Δt. However, unlike the Sup35 peptide, which undergoes relatively small fluctuations in $\beta(t)$ after it forms in registry β-strand, the Aβ peptide undergoes substantial changes in $\beta(t)$ (Fig. 1*D*) despite being simulated at a lower temperature (T = 290 K) compared with the Sup35 peptide (T = 330 K). In one of the trajectories, the Aβ peptide repeatedly samples $\beta(t) \approx 0.6$, which shows that the landscape for the Aβ peptide aggregation is rugged. We show below that the large conformational fluctuation observed in the Aβ peptides is related to the substantial stability differences between the 2 fibril structures.

Dynamics of Intramolecular Steric Zipper Formation in the Sup35 Fibril Is Heterogeneous at the Molecular Level. The amyloid crystal structures (4) show that the interface between the 2 adjacent β-sheets in the Sup35 fibril that are within 5–8 Å (Fig. 1*A*) is dry except in the vicinity of the carboxylate ions. However, there is no water present between the parallel β-strands within a single sheet (ones shown in purple in Fig. 1*A*, for example). To probe the dynamics of addition of in-register formation of the locking monomer, with concomitant increase in the β-strand content, we have calculated the time-dependent changes in the distance between the centers of mass of the side chains of the solvated monomer and the underlying fibril monomers, $d_{jl}(t)$ (j refers to the side chain of the solvated monomer, and l labels the identical residue in the underlying fibril). The results in Fig. 2 show that, despite the overall cooperativity in the enhancement of $\beta(t)$ (Fig. 1*C*), the decrease in $d_{jl}(t)$ (j and l range from 2 to 7), occurs over a broad spectrum of times. In the trajectory (Fig.

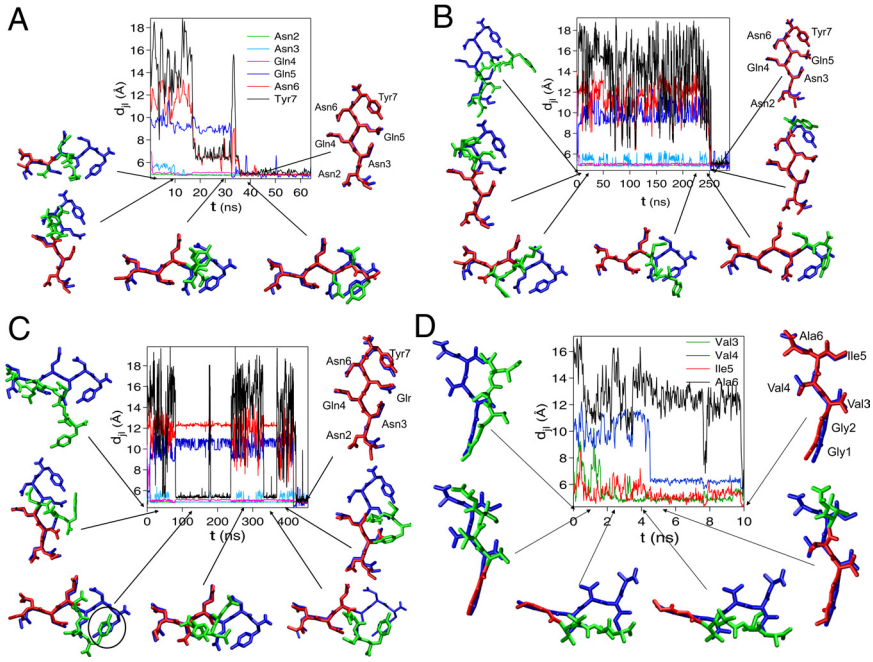

Fig. 2. Time evolution of the side-chain center of mass distance, d_{jl}, between the in-register residues of the locking Sup35 and Aβ monomers and its neighbor in the same β-sheet. (*A–C*) The 3 trajectories for the Sup35 fibril growth. Residues 2–7 are plotted: Asn-2 (green), Asn-3 (light blue), Gln-4 (purple), Gln-5 (blue), Asn-6 (red), Tyr-7 (black). Side chains of residues 2–4 in the Sup35 monomer lock in <10 ns. Residues 5–7 take a longer time and form in-register contacts simultaneously. (*D*) Same as *A–C* except that the graph is for the Aβ fibril growth in 1 trajectory. The colors correspond to Val-3 (green), Val-4 (light blue), Ile-5 (red), Ala-6 (black). The crystal monomer is shown in blue in *A–D*. Part of the monomer locked onto the crystal is shown in red, and part of the unlocked monomer is in green.

2*A*) with the shortest first-passage time, the 2 Asp and the Gln residues from the C terminus interlock rapidly (≈10 ns). The full intrasheet steric zipper, in which all 7 residues are in perfect registry, forms in ≈50 ns. In contrast, the time for forming the steric zipper can be long (≈400 ns) as shown in Fig. 2*C*. There is also heterogeneity in the locking of the individual residues that result in tight packing. For example, the order of decrease in $d_{jl}(t)$ in Fig. 2 *A* and *B* are somewhat similar. On a short time scale, N2, N3, and Q4 residues of the solvated monomer interdigitate perfectly with their counterparts in the fibril (Fig. 2 *A* and *B*). The interdigitation is also shown in terms of the structures in which residues in red (solvated) monomer are superimposed on the underlying residues in blue from the fibril. The residues in green are not in registry, and the values of $d_{jl}(t)$ are large for $t < \tau_i$, the first-passage time for trajectory *i*. The remaining residues (Q5, N6, and Y7) achieve their fibrillar conformation at $t \approx \tau_i$ nearly simultaneously (Fig. 2 *A* and *B*).

The dynamics of intramolecular zipper formation is dramatically different in the third trajectory (Fig. 2*C*). In this case, just as in Fig. 2 *A* and *B*, the 3 N-terminal residues adopt the fibril-compatible structure on a rapid time scale. Interestingly, the aromatic ring in Y7 contacts its counterpart in the underlying lattice at $t \approx 100$ ns (Fig. 2*C*). However, the orientation of the ring is flipped (see the circle portion of the snapshot in Fig. 2*C*). After repeated association and dissociation, which results in an increase of $d_{77}(t)$ (Fig. 2*C*), the 3 residues interdigitate at $t \approx \tau_i$ to complete the formation of in register parallel strand. The formation of near-native contact between the 2 Tyr residues and the subsequent reversal before the completion of locking is reminiscent of "backtracking" in the folding of the large protein interleukin (40). The diversity in the time scale, and presumably in the routes in the locking process, although inferred from only a few trajectories, is plausibly a characteristic of heterogeneous growth of amyloid fibrils.

In contrast to the growth of the Sup35 fibrils, the locking of the Aβ monomer to the fibril lattice is very rapid (Fig. 2*D*). The hydrophobic association between the 2 Aβ strands occurs rapidly, indicating that the expulsion of water is an early event. However, the stability of the locked Aβ peptide is less than the Sup35 monomer, which results in large conformational fluctuations of Aβ monomer (see below).

Peptide Assimilation Involves Excursion Through Metastable States. Time-dependent changes in the nematic order parameter (P_2, Eq. **1** in *SI Text*) show that the soluble monomer hops through a number of metastable states before adopting in-registry β-strand conformation (Fig. 3). The formation of metastable structures can be traced to intermolecular hydrogen bonding and steric interactions between the locking monomer and the underlying fibril. The backbone and side chains of the monomer residues ^{3}NQQN^6 form interpeptide hydrogen bonds with the fibril at positions that are not commensurate with the ordered structure. The formation of these favorable, but nonnative, interactions have to be disrupted for the monomer to escape from the metastable kinetic traps. The jump times between the metastable structures as well as the transition to the ordered state are much shorter than their lifetimes (Fig. 3*A*). Upon formation of the locked state, the monomer is stabilized by backbone and side-chain intermolecular interactions.

The nature of metastable states and the associated lifetimes are drastically different in the process of addition of Aβ peptide to a growing fibril (Fig. 3*B*). The nonpolar side chains of the Aβ peptide, which interact with the fibril largely through weak hydrophobic interactions, cannot form hydrogen bonds. Because of weak dispersion interactions associated with the Aβ peptides the metastable interactions can be easily disrupted. Consequently, the lifetimes of the metastable states are short, enabling rapid hopping between the various states (Fig. 3*B*). This behavior of Aβ peptide stands in contrast to that of the Sup35 monomer, which can be trapped in metastable intermediates for long times. Although the initial locking and transition between the metastable structures are rapid in the case of Aβ monomers, interpeptide steric interactions can prevent in-register β-strand formation (Fig. S2). The nematic order parameter for one of the trajectories shows that, even after 0.1 μs, the value of $P_2 \approx 0.6$. In this state (Fig. S2), 4 residues adopt correct

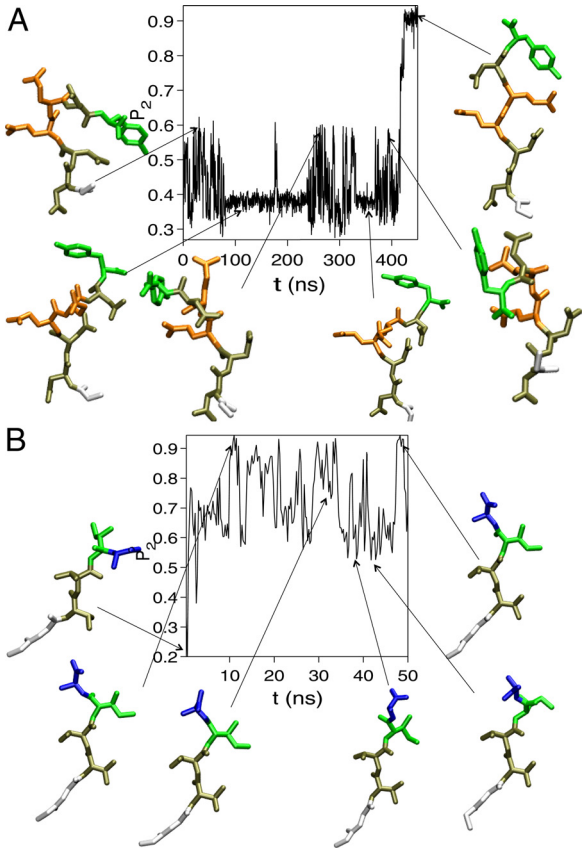

Fig. 3. Time-dependent changes in the nematic order parameter (see *SI Text*). (*A*) Sup35 monomer. The locked Sup35 monomer is stabilized through backbone and side-chain intermolecular hydrogen bonds in addition to the hydrophobic interactions. (*B*) Aβ monomer. The locked Aβ monomer fluctuates as it is stabilized only through weak dispersion interactions.

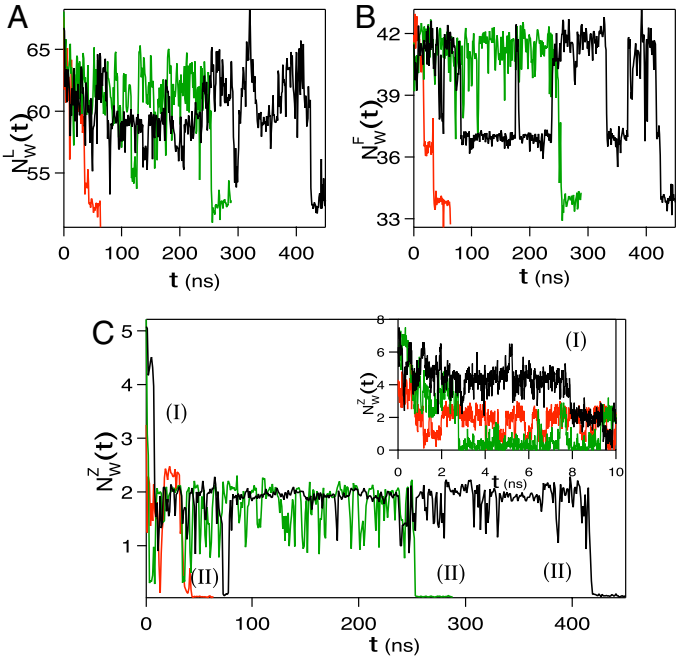

Fig. 4. Role of water molecules in the addition reaction in the 3 MD trajectories. (*A*) Dynamical changes in the number of water molecules near the Sup35 monomer as it locks onto the fibril. (*B*) Variations in the number of water molecules that are in the neighborhood of the fibril monomer onto which the Sup35 monomer docks and locks (in Fig. 1*A*), viewing from the top, the first monomer in the β-strand shown in silver color). (*C*) Time-dependent changes in the number of water molecules in the zipper region. Water in the zipper region is expelled in 2 distinct stages. In stage I as shown in the *Inset*, there are ≈7–9 water molecules at the start of the lock phase, and the number decreases to ≈2 in 10 ns. In stage II, water molecules are completely expelled as the monomer locks onto the fibril. The number of water molecules is averaged over a time period of 1 ns in all of the 3 plots except that in the *Inset* it is averaged over 10 ps. In *A*–*C*, only water molecules that are within 3.5 Å of the peptide are considered.

positions, whereas residues 5 and 6 form nonnative contacts (that are absent in the amyloid fibril). The escape from this structure requires partially unzipping of the correctly formed contacts, which requires overcoming a large free-energy barrier.

Two-Stage Dehydration and the Locking Process Are Coincident for the Sup35 Peptide. The number of water molecules, averaged over time, $N_W(t) = \frac{1}{\Delta}\int_t^{t+\Delta} N_W(s)ds$ ($\Delta = 1$ ns), in the vicinity of both the Sup35 and Aβ monomers decreases as the interaction with the underlying fibril lattice increases (Figs. 4*A* and 5*A*). As the locking reaction progresses, water molecules in the vicinity of the monomer in the fibril that are closest to the solvated monomer (the first β-strand shown in silver in Fig. 1) are expelled (Figs. 4*B* and 5*B*). Comparison of the dynamics associated with the Aβ and Sup35 locking shows that the dehydration process is dynamically more cooperative in the locking of the Sup35. For both Sup35 and Aβ monomers, fluctuations in the number of water molecules coincide with the locking events (see Figs. 3 and 4). The largest fluctuations in the number of water molecules near the locking monomer, $N_W^L(t)$, and the solvent-exposed monomer in the fibril, $N_W^F(t)$, occurs exactly when the monomer completely locks into the crystal cooperatively (Fig. 4 *A* and *B*). The coincidence of the locking step and dehydration is also reflected in the sharp, almost stepwise, decrease in the water content in the zipper region of the Sup35 crystal (Fig. 4*C*). The number of water molecules, $N_W^Z(t)$, decreases abruptly from 8 to 2 as the docking is initiated, and finally goes to zero as the locking process is complete (Fig. 4*C*). These observations show that dehydration, resulting in the formation of the dry zipper region (4) as the monomer locks into the fibril lattice, is a key event in the growth of the amyloid fibrils. We surmise that interactions involving water must play an important role in the rate of fibril growth (41, 42).

Rapid Locking Requires Formation of Native-Like Contacts During the Docking Stage. The results presented so far are based on simulations that were initiated by forming a transient native contact between the Gly of the unstructured monomer with the underlying fibril, which was needed to observe the growth process in the time scale of the simulations. To assess the role of the initial conformations on the dynamics of the monomer assimilation step, we also performed multiple simulations by harmonically constraining the center of mass of the Sup35 monomer to the fibril surface to facilitate docking of the peptide. The peptide docks onto the fibril lattice within 50 ps (see the *Inset* to Fig. S3) after which the harmonic constraint is removed. In 3 of the 4 long trajectories, the docked monomer unbinds from the fibril within ≈70 ns (see Fig. S3). In one of the trajectories, an incorrect but stable native-like contact between Q5 of the docked monomer and Q4 of the monomer in the underlying fibril lattice forms relatively early. After nearly 300 ns, fluctuations drive the monomer from the fibril surface (Fig. S3). These simulations suggest that template-mediated assembly of the docked monomer and the fibril might involve a number of undocking/docking events before assimilation onto the growing fibril. The time scale for growth of the fibril depends critically on the nature of the ensemble of molecules that are generated at the end of the docking process. It appears that only a small fraction of monomers,

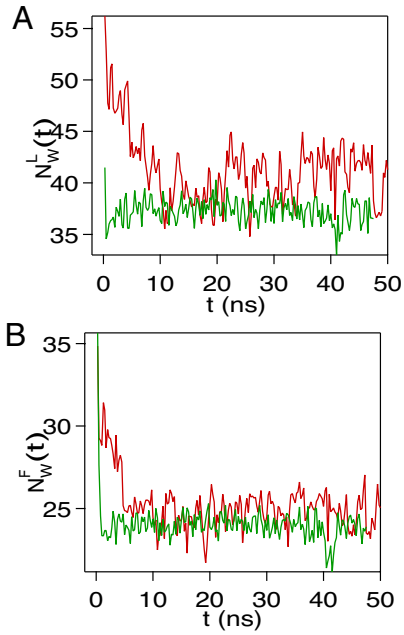

Fig. 5. Changes in the number of water molecules within 3.5 Å of the Aβ peptides as a function of time. (*A*) $N_W^L(t)$ is the number of waters around the locking Aβ monomer. (*B*) $N_W^F(t)$ shows water molecules that are near the closest neighbor in the fibril to the locking monomer (in Fig. 1*B*, viewing from the top, the first monomer in the β-strand shown in silver color). The number of water molecules is averaged over a time period of 1 ns.

which establish at least 1 native-like interaction with the monomer in the fibril, can rapidly lock and assimilate onto the fibril.

Favorable Electrostatic and Dispersion Interactions Stabilize Sup35 Fibrils to a Greater Extent than Aβ Fibrils. The greater dynamic cooperativity of the locking process of the addition of Sup35 monomer to the fibril compared with the growth of Aβ fibril is also reflected in the interactions that stabilize the 2 fibrils. We computed the electrostatic (V_{ee}) and van der Waals interaction (V_{vdw}) energies between the neighboring monomers in the Sup35 and Aβ fibrils (Table S1) show that V_{ee} associated with the monomers in the Sup35 fibril is more favorable than in the Aβ fibrils because the side chains of the 5 polar residues (^{2}NNQQN^6) in the Sup35 peptide can form a tight network of inter peptide hydrogen bonds. In addition, the van der Waals interaction between the monomers in the Sup35 crystal is also considerately more favorable than in the Aβ fibrils (Table S1). In the parallel arrangement of the β-strands, the contacts between the nonpolar groups in N, Q, and Y lead to favorable dispersion interactions. Six residues in the Sup35 peptide have nonpolar groups, whereas in the Aβ monomer, there are only 4 small nonpolar residues (^{3}VVIA^6). Moreover, the inability of the side chains in the Aβ monomer to form interpeptide hydrogen bonds, which orientationally pins the Sup35 peptide on the fibrils, leads to a less-stable microcrystal. As a result, there are greater conformational fluctuations in the Aβ fibrils even after the locking process is complete (Fig. 3*B*).

Sup35 Fibrils Can Be Destabilized by Ala Mutations. To further illustrate the effect of the interpeptide side-chain hydrogen bonds on the stability of the Sup35 fibrils, we probed the dynamic stability of the ordered state by performing Ala scanning mutations (24) (Fig. S4). Four mutants M1 (residue 4), M2 (residues 4 and 6), M3 (residues 2, 4, and 6), and M4 (residues 2–6), in which the residues in parentheses were replaced by Ala, were studied. The time-dependent root mean-square deviations, Δ(*t*), from the WT shows that M1 (residue 4) and M2 (residues 4 and 6) are nearly as stable as the WT crystals. Although, the zipper contacts and the amide–amide hydrogen bonds in the β-sheet, formed by residues Q and N with the WT, are disrupted in the mutants, the docked mutant monomer in the crystal is stabilized by backbone hydrogen bonds and side-chain amide hydrogen bonds formed by N2, N3, and Q5. In M3 (residues 2, 4, and 6). all of the zipper contacts and amide–amide hydrogen bonds on the zipper side are disrupted, which makes M3 (residues 2, 4, and 6) flexible in the crystal. As a result, the value of Δ(*t*) increases. Finally, in M4 (residues 2–6), there is a complete loss of amide–amide stacking hydrogen bonds and zipper contacts. Increasing the hydrophobic interactions between the monomers without compensating for the loss of hydrogen bonds renders the Sup35 fibrils unstable. These calculations also show that the greater stability of the peptides in the Sup35 fibril, relative to the Aβ fibrils, is due to enhanced orientational ordering resulting from hydrogen bond formation.

Concluding Remarks

Extensive all-atom MD simulations of the addition of the unstructured monomers (GNNQQNY from Sup35 and GGVVIA from the Aβ peptide) to the end of the amyloid fibril show that the process of locking is dynamically cooperative (Fig. 1). The assembly process is heterogeneous at the molecular level, especially for the addition of the Aβ peptide to the fibril. Conformational fluctuations after the Sup35 monomer adopts the β-strand conformation are much smaller than those observed for the Aβ monomer. Interpeptide hydrogen bonds between adjacent β-strands in the Aβ fibril fluctuate greatly on a time scale on the order of a few nanoseconds. Time-dependent changes in the hydrogen bonds between β-strands in the Sup35 fibril occur much more cooperatively in an all-or-none manner (Fig. S5). The differences, which are reflected in the stability of amyloid fibrils, result in larger conformational fluctuations in the Aβ fibrils compared with the Sup35 structure.

Before the addition of the monomer to the underlying fibril, the strands on the fibril form hydrogen bonds with the water molecules. As the locking reaction progresses, water molecules are expelled, and the interactions are replaced by the in-register interactions with the β-strand of the fibril. Drying of the interface between 2 adjacent β-strands in the fibril occurs in 2 distinct steps. In the initial rapid stage, there is a sharp decrease in the number of interfacial water molecules as the monomer docks on the fibril. Complete dehydration resulting in a dry environment between the β-sheet and the formation of a parallel strand arrangement occurs simultaneously, especially in the addition of GNNQQNY on to the Sup35 fibril. The remarkably cooperative expulsion of a number of water molecules over a very short time, which occurs late in the assembly process, shows that it is an essential step in stabilizing the amyloid fibril.

From a global perspective, the mechanisms of amyloid fibril growth appear to be similar. However, comparison of the molecular processes involved in the addition of the NQ-rich peptide and the hydrophobic Aβ peptide to their respective fibrils reveals crucial differences in the dynamics of addition and the nature of interaction that stabilize the ordered state. In the case of GNNQQNY fibrils, precise in-register interactions between the side chains of the monomers renders the interface dry. More importantly, as noted previously (4, 44), a network of hydrogen bonds involving the backbone and side chains across the dry interface further stabilizes the β-sheets. Our simulations show that the dynamics of the network of hydrogen bonds, which is analogous to the Perutz polar zipper model (43) for fibrils involving glutamine repeats, changes coherently across the interface. Indeed, the ability to form the network of hydrogen bonds (Fig. S6) makes the GNNQQNY fibrils considerably more stable than the Aβ fibrils. The fibrils from Aβ-peptides are largely held together by the much weaker and nonspecific dispersion interactions between the hydrophobic side chains. Consequently, the Aβ fibrils are much less stable and undergo substantial fluctuations even after the locking process is

complete. Taken together, these results show that the fibril stability can be enhanced by stitching together β-sheets with hydrogen bonds involving both the backbone and side chains. If the Sup35 peptide chains are mutated to Ala, the stability of the fibril is compromised. This observation further emphasizes the importance of the network of hydrogen bonds. Decomposition of the stabilization energy of the Sup35 and Aβ fibril suggests that the electrostatic (network of hydrogen bonds) are crucial in enhancing the stability of the Sup35 fibrils. We speculate that sequences that can form a large network of interpeptide hydrogen bonds lead to fibrils with enhanced stability. Our work also suggests that the rate of growth of fibrils could increase as the stability of the fibril decreases.

Methods

Models. The crystal structures of the fibrils of the heptapeptide ^{7}GNNQQNY^{13}, from the yeast prion protein Sup35, and the hexapeptide ^{37}GGVVIA^{42}, from the Aβ protein, belong to 2 different classes (4, 5). In the ordered state, the surfaces of the 2 different β-strands interlock to form a steric zipper structure in which the side chains of each β-sheet face at the interface, interdigitate into one another. In the microcrystal of GNNQQNY (referred to as Sup35 fibril here), identical surfaces of the β-strands interact to form the zipper region, whereas in the Aβ fibril, different surfaces interact to form the zipper region. In the Sup35 fibril, identical edges of the monomers in 2 different β-strands point in the same direction (up–up) (5), whereas in the Aβ fibril they point in different directions (up–down). Our simulations (see *SI Text* for details and analysis) use the amyloid structures as the starting point for probing the dynamics of the growth process.

Initial Conformations. We first created a protofilament with a vacancy (Fig. 1*A*) that results in a terrace-like shape on the crystal. The vacancy is created by initially restraining all but 1 of the strands (the gray strand in Fig. 1) to their fibril structures. The system is heated to $\approx$1,000 K, which results in dissociation of the strand, leaving a step-like vacancy. From the high-temperature simulations, conformations where the dissociated monomer is in proximity (where 1 of the residues interacting with the fibril lattice) to the underlying fibril are chosen as the starting structures. One of the β-sheets of the protofilament (purple in Fig. 1*A*) has 3 β-strands, whereas the other has 2 (silver in Fig. 1*A*). A solvated monomer can dock and lock onto the crystal. Because the time scale for monomer addition is long (milliseconds to seconds), we describe the structural transition in the locking step of the monomer after contact with the protofibril is initiated. In most cases, we began the simulations with the monomer having the Gly initially in contact with the crystal. At subsequent times, there are no restraints between the monomer and the fibril. Four independent simulation trajectories, for an accumulated time of 0.8 μs for the addition of the Sup35 peptide to the underlying crystal were generated. We use the same procedures to simulate the locking of the Aβ monomer into the crystal (Fig. 1*B*). Three independent trajectories of the Aβ monomer locking into the crystal were generated. The total simulation time of the 3 trajectories is $\approx$0.23 μs (see Table S2 for details).

ACKNOWLEDGMENTS. This work was supported in part by a grant from the National Institutes of Health through Grant R01GM076688-05. A portion of this research was conducted at the Center for Nanophase Materials Sciences, which is sponsored at Oak Ridge National Laboratory by the Division of Scientific User Facilities, U.S. Department of Energy through Grant CNMS2007-048. Part of the computational work was done by using the resources of National Science Foundation Teragrid through Grant TG-MCB080035N.

1. Chiti F, Dobson CM (2009) Amyloid formation by globular proteins under native conditions. *Nat Chem Biol* 5:15–22.
2. Bennett MJ, Sawaya MR, Eisenberg D (2006) Deposition diseases and 3D domain swapping. *Structure (London)* 14:811–824.
3. Thirumalai D, Klimov DK, Dima RI (2003) Emerging ideas on the molecular basis of protein and peptide aggregation. *Curr Opin Struct Biol* 13:146–159.
4. Nelson R, et al. (2005) Structure of the cross-β spine of amyloid-like fibrils. *Nature* 435:773–778.
5. Sawaya MR, et al. (2007) Atomic structures of amyloid cross-β spines reveal varied steric zippers. *Nature* 447:453–457.
6. Tycko R (2006) Molecular structure of amyloid fibrils: Insights from solid-state NMR. *Quart Review Biophys* 39:1–55.
7. Petkova AT, Yau WM, Tycko R (2006) Experimental constraints on quaternary structure in Alzheimer's beta-amyloid fibrils. *Biochemistry* 45:498–512.
8. Ma B, Nussinov R (2002) Stabilities and conformations of Alzheimer's β-amyloid peptide oligomers (Aβ_{16-22}, A$\beta_{16-35}$and Aβ_{10-35}): Sequence effects. *Proc Natl Acad Sci USA* 99:14126–14131.
9. Paravastua AK, Leapman RD, Yau WM, Tycko R (2008) Molecular structural basis for polymorphism in Alzheimer's beta-amyloid fibrils. *Proc Natl Acad Sci USA* 105:18349–18354.
10. Xue WF, Homans SW, Radford SE (2008) Systematic analysis of nucleation-dependent polymerization reveals new insights into the mechanism of amyloid self-assembly. *Proc Natl Acad Sci USA* 105:8926–8931.
11. Harper JD, Lansbury PT (1997) Models of amyloid seeding in Alzheimer's disease and scrapie: Mechanistic truths and physiological consequences of time-dependent stability of amyloid proteins. *Annu Rev Biochem* 66:385–407.
12. Serio TR, et al. (2000) Nucleated conformational conversion and the replication of conformational information by a prion determinant. *Science* 289:1317–1321.
13. Collins SR, Douglass A, Vale RD, Weissman JS (2004) Mechanism of prion propagation: Amyloid growth occurs by monomer addition. *PLOS Biol* 2:1582–1590.
14. Klimov DK, Thirumalai D (2003) Dissecting the assembly of Aβ_{16-22} amyloid peptides into antiparallel β sheets. *Structure (London)* 11:295–307.
15. Gsponer J, Haberthur U, Caflisch A (2003) The role of side-chain interactions in the early steps of aggregation: molecular dynamics simulations of an amyloid-forming peptide from the yeast prion Sup35. *Proc Natl Acad Sci USA* 100:5154–5159.
16. Santini S, Mousseau N, Derreumaux P (2004) In silico assembly of Alzheimer's Aβ_{16-22} peptide into β-sheets. *J Am Chem Soc* 126:11509–11516.
17. Santini S, Wei G, Mousseau N, Derreumaux P (2004) Pathway complexity of Alzheimer's β-amyloid Aβ_{16-22} peptide assembly. *Structure (London)* 12:1245–1255.
18. Gnanakaran S, Nussinov R, Garcia AE (2006) Atomic-level description of amyloid β-dimer formation. *J Am Chem Soc* 128:2158–2159.
19. Nguyen PH, Li MS, Stock G, Straub JE, Thirumalai D (2007) Monomer adds to a preformed structured oligomers of Aβ-peptides by a two-stage dock-lock mechanism. *Proc Natl Acad Sci USA* 104:111–116.
20. Zhang Z, Chen H, Bai H, Lai L (2007) Molecular dynamics simulations on the oligomer-formation process on the GNNQQNY peptide from yeast prion protein Sup35. *Biophys J* 93:1484–1492.
21. Meli M, Morra G, Colombo G (2008) Investigating the mechanism of peptide aggregation: Insights from mixed Monte Carlo-molecular dynamics simulations. *Biophys J* 94:4414–4426.
22. Irback A, Mitternacht S (2008) Spontaneous β-barrel formation: An all-atom Monte Carlo study of Aβ_{16-22} oligomerization. *Proteins* 71:207–214.
23. Strodel B, Whittleston CS, Wale DJ (2007) Thermodynamics and kinetics of aggregation for the GNNQQNY peptide. *J Am Chem Soc* 129:16005–16014.
24. Zheng J, Ma B, Tsai CJ, Nussinov R (2006) Structural stability and dynamics of an amyloid-forming peptide GNNQQNY from the yeast prion sup-35. *Biophys J* 91:824–833.
25. Smith AV, Hall CK (2001) Protein refolding versus aggregation: Computer simulations on an intermediate-resolution protein model. *J Mol Biol* 312:187–202.
26. Nguyen HD, Hall CK (2005) Kinetics of fibril formation by polyalanine peptides. *J Biol Chem* 280:9074–9082.
27. Orte A, et al. (2008) Direct characterization of amyloidogenic oligomers by single-molecule fluorescence. *Proc Natl Acad Sci USA* 105:14424–14429.
28. Lux Fawzi N, Okabe Y, Yap EH, Head-Gordon T (2007) Fibril stability and elongation studies of the Alzheimer's Aβ1–40 peptide. *J Mol Biol* 365:535–550.
29. Bellesia G, Shea JE (2007) Self-assembly of beta-sheet forming peptides into chiral fibrillar clusters. *J Chem Phys* 126:245104–245111.
30. Li MS, Klimov DK, Straub JE, Thirumalai D (2008) Probing the mechanism of fibril formation using lattice models. *J Chem Phys* 129:175101–175110.
31. Bellesia G, Shea JE (2009) Effect of β-sheet propensity on peptide aggregation. *J Chem Phys* 130:145103–145110.
32. Pellarin R, Guarnera E, Calfisch A (2007) Pathways and intermediates of amyloid fibril formation. *J Mol Biol* 374:917–924.
33. Esler WP, et al. (2000) Alzheimer's disease amyloid propagation by a template-dependent dock-lock mechanism. *Biochemistry* 39:6288–6295.
34. Gobbi M, et al. (2006) Gerstmann–Strarussler–Scheinker disease amyloid protein polymerizes according to the dock-and-lock model. *J Biol Chem* 281:843–849.
35. Massi F, Straub JE (2001) Energy landscape theory for Alzheimer's amyloid β-peptide fibril elongation. *Proteins* 42:217–226.
36. Onuchic JN, Wolynes PG (2004) Theory of protein folding. *Curr Opin Struct Biol* 14:70–75.
37. Thirumalai D, Hyeon C (2005) RNA and protein folding: Common themes and variations. *Biochemistry* 44:4957–4970.
38. Lipfert J, Franklin J, Wu F, Doniach S (2005) Protein misfolding and amyloid formation for the peptide GNNQQNY from yeast prion protein Sup35: Simulation by reaction path annealing. *J Mol Biol* 349:648–658.
39. Frishman D, Argos P (1995) Knowledge-based protein secondary structure assignment. *Proteins* 23:566–579.
40. Gosavi S, Chavez LL, Jennings PA, Onuchic JN (2006) Topological frustration and the folding of Interleukin. *J Mol Biol* 357:986–996.
41. Krone M, et al. (2008) Role of water in mediating the assembly of Alzheimer amyloid-β Aβ(16–22) protofilaments. *J Am Chem Soc* 130:11066–11072.
42. Mukherjee A, Chowdhury P, Gai F (2009) Effect of dehydration on the aggregation kinetics of two amyloid peptides. *J Phys Chem B* 113:531–535.
43. Perutz MF, Pope BJ, Owen D, Wanker EE, Scherzinger E (2002) Aggregation of proteins with expanded glutamine and alanine repeats of the glutamine-rich and asparagine-rich domains of Sup35 and of the amyloid β-peptide of amyloid plaques. *Proc Natl Acad Sci USA* 99:5596–5600.
44. Tsemekhman K, Goldschmidt L, Eisenberg D, Baker D (2007) Cooperative hydrogen bonding in amyloid formation. *Prot Sci* 16:761–764.